Active Stabilization of the Resistive-Wall Mode in High-Beta, Low-Rotation Plasmas

S. A. Sabbagh,[1] R. E. Bell,[2] J. E. Menard,[2] D. A. Gates,[2] A. C. Sontag,[1] J. M. Bialek,[1] B. P. LeBlanc,[2] F. M. Levinton,[3] K. Tritz,[4] and H. Yuh[3]

[1]*Department of Applied Physics and Applied Mathematics, Columbia University, New York, New York 10027, USA*
[2]*Princeton Plasma Physics Laboratory, Princeton University, Princeton, New Jersey 08543, USA*
[3]*Nova Photonics, Princeton University, Princeton, New Jersey 08543, USA*
[4]*Johns Hopkins University, Baltimore, Maryland 21218, USA*

(Received 4 June 2006; published 28 July 2006)

The resistive-wall mode is actively stabilized in the National Spherical Torus Experiment in high-beta plasmas rotating significantly below the critical rotation speed for passive stability and in the range predicted for the International Thermonuclear Experimental Reactor. Variation of feedback stabilization parameters shows mode excitation or suppression. Stabilization of toroidal mode number unity did not lead to instability of toroidal mode number two. The mode can become unstable by deforming poloidally, an important consideration for stabilization system design.

DOI: 10.1103/PhysRevLett.97.045004 PACS numbers: 52.35.Py, 52.55.Fa, 52.55.Tn, 52.65.Kj

Large scale magnetohydrodynamic (MHD) instabilities impose significant limits to fusion power production in magnetic fusion plasmas. A formidable example is the long wavelength kink-ballooning instability which grows on the rapid Alfvén time scale and typically leads to plasma pressure collapse and current disruption. This mode rotates along with a rotating plasma and may be stabilized by the presence of an electrically conducting wall, but can result in the destabilization of the resistive-wall mode (RWM) [1,2], a branch of the kink instability that grows on the relatively slow eddy current decay time of the resistive wall, τ_w. The RWM is amenable to passive stabilization [1,3,4] that theoretically occurs due to energy dissipation related to plasma rotation [5]. At sufficiently high plasma pressure in relation to the confining magnetic field (toroidal and normalized plasma beta, $\beta_t \equiv 2\mu_0\langle p\rangle/B_0^2$ and $\beta_N \equiv 10^8\langle\beta_t\rangle aB_0/I_p$) and at plasma toroidal rotation speeds, ω_ϕ, below a critical value, $\Omega_{\rm crit}$, the RWM becomes unstable. Here, p is the plasma pressure, B_0 is the vacuum toroidal field at the plasma geometric center, a is the plasma minor radius at the midplane, I_p is the plasma current, and brackets represent volume average. RWM destabilization can occur when β_N exceeds $\beta_{N(n)}^{\text{no-wall}}$, the value where ideal MHD modes with toroidal mode number, n, become unstable with no stabilizing wall present. In this Letter, $\beta_N^{\text{no-wall}} \equiv \beta_{N(n=1)}^{\text{no-wall}}$. The $\Omega_{\rm crit}$ is usually quoted at low integer values of the plasma safety factor, q (typically, $q = 2$), normalized to the Alfvén frequency, ω_A, and $\Omega_{\rm crit}/\omega_A$ is typically one to a few percent [6,7]. Generally, the larger plasma rotation profile is important in determining RWM stability [4,7,8], so $\Omega_{\rm crit}$ is more appropriately expressed as a profile rather than a scalar. Confirmation of RWM passive stabilization physics is still an active area of research.

RWM active stabilization can be used when ω_ϕ is insufficient for passive stabilization and is expected to be required for burning fusion plasmas in the International Thermonuclear Experimental Reactor (ITER) [9] operating in high performance scenarios [7]. Active stabilization has been addressed to stabilize pressure-driven modes in rotating tokamak plasmas [10–12] and current-driven modes in reversed-field pinches [13]. Present tokamak research now focuses on active stabilization of the $n = 1$ RWM at low levels of ω_ϕ [12]. Stabilization is typically realized by a feedback control loop consisting of magnetic sensors capable of detecting low frequency $\sim O(1/\tau_w)$ modes, a set of control coils to provide magnetic field in response to the detected modes, and a control algorithm that determines the form of the response. Control algorithms aim to approximately eliminate the dominant measured field asymmetry [14]. Tokamak experiments presently focus on stabilizing RWMs with $n = 1$ since they minimize field line bending and are usually the least stable. Important corollary research includes how the RWM reacts to stabilization, including the behavior of $n > 1$ modes in this condition.

The present study demonstrates for the first time active stabilization of the pressure-driven RWM in high-beta, low aspect ratio tokamak plasmas, with ω_ϕ significantly below the entire critical rotation profile. The low aspect ratio ($A \equiv R_0/a$, where R_0 is the major radius) configuration, or spherical torus, produces high β_t and energy confinement, τ_E, advanced tokamak equilibria with broad pressure and current (low plasma internal inductance, l_i) profiles most amenable to kink and RWM stabilization. The experiments were performed in the National Spherical Torus Experiment (NSTX) [15], recently outfitted with an RWM active stabilization system. Current ramping to decrease l_i or other techniques to reduce $\beta_N^{\text{no-wall}}$ used to excite RWM growth in tokamaks [12] were not required. The role of the $n = 2$ RWM during active $n = 1$ stabilization can be readily studied, since the device is equipped to

measure up to $n = 3$, and unstable RWMs with $n = 1$–3 have already been observed in NSTX [4]. Plasma rotation is measured at 51 major radial locations at the device midplane by a charge exchange recombination spectroscopy diagnostic using emission from C^{5+} at 5290 Å. Toroidally directed neutral beam injection power, P_b, used to heat the plasma normally produces high plasma rotation, which has reached values of $\omega_\phi/\omega_A = 0.48$ [4]. Plasma toroidal rotation was controlled by the application of nonresonant, $n = 3$ magnetic braking [16], reducing ω_ϕ significantly below $\Omega_{\rm crit}$, and in the predicted range of $\omega_\phi/\Omega_{\rm crit}$ for ITER plasmas. The present results have important ramifications for the design of RWM stabilization systems planned for future devices such as ITER and the Korean Superconducting Tokamak Advanced Research device (KSTAR) [17].

A comparison of high β_N plasmas with and without RWM active stabilization is shown in Fig. 1. All discharges have constant $P_b = 6.3$ MW. The plasma without active stabilization has $\beta_N = 4.1$ as $\omega_\phi/2\pi$ at major radial position $R = 1.323$ m (near the $q = 2$ flux surface) drops to below 4 kHz. At this time, RWM passive stabilization becomes insufficient and the $n = 1$ RWM becomes unstable, indicated by poloidal and radial field sensors (ΔB_p, $\Delta B_{r-\rm ext}$), and β_N collapses. With active stabilization turned off, the current in one of three control coil pairs, I_A, is the preprogrammed $n = 3$ braking field current [Fig. 1(c)]. The experimentally fitted $n = 1$ RWM growth rate is between 0.5–0.25 s^{-1}. This agrees well with the theoretical growth rate $\gamma_{\rm RWM} = 0.37$ s^{-1} as computed by the VALEN-3D code [18], using experimental equilibrium reconstructions [19] including internal magnetic field pitch angle constraints from a motional Stark effect diagnostic. In contrast, the plasma with active stabilization does not suffer an unstable RWM and continues to increase in β_N up to 5.6 and β_t up to 19.4%, as ω_ϕ continues to decrease to $\omega_\phi/\Omega_{\rm crit} = 0.2$ near $q = 2$. The RWM is actively stabilized above $\beta_N^{\rm no\text{-}wall}$ and below $\Omega_{\rm crit}$ for significantly long duration exceeding $90/\gamma_{\rm RWM}$ and seven τ_E. The time evolution of $\beta_N^{\rm no\text{-}wall}$ is computed by the DCON MHD stability code [20]. The control coil current is now the superposition of the $n = 3$ braking field current and the $n = 1$ active feedback stabilization current, which is determined by the measured $n = 1$ RWM amplitude and phase. This amplitude, $\Delta B_{pu}^{n=1}$, measured by an array of 12 poloidal field sensors above the device midplane, includes both the RWM field as well as the field generated by mode-induced eddy currents in the passive stabilizing plates. The amplitude modulation shown in Fig. 1(d) is attributed to the interaction of the mode and eddy current fields. The field generated by I_A is subtracted from $\Delta B_{pu}^{n=1}$. The $\Delta B_{pu}^{n=1}$ is larger in the nonstabilized plasma as the $n = 1$ RWM becomes unstable, and in the stabilized plasma is controlled at an average level of about 5 G. During $n = 1$ stabilization, the $n = 2$ RWM does not become unstable, although $\Delta B_{pu}^{n=2}$ becomes larger than $\Delta B_{pu}^{n=1}$ at the lowest values of ω_ϕ and highest values of β_N [Fig. 1(e)]. The actively stabilized, low ω_ϕ plasmas can suffer partial β_N collapse due to largely internal modes, which do not disrupt I_p, allowing β_N to recover. An example is shown by the dotted curves in Fig. 1. DCON stability calculations show that $\beta_N > \beta_{N(n=2)}^{\rm no\text{-}wall}$ and are consistent with the identification of this mode as an $n = 2$ internal MHD instability. Further details of this mode will be shown in Fig. 4.

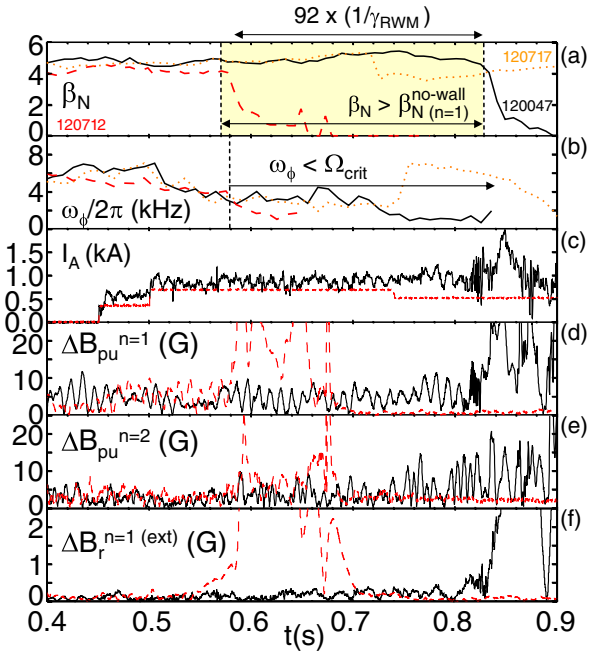

FIG. 1 (color online). RWM active feedback stabilization in low-rotation plasmas. Solid curves, actively stabilized plasma at ω_ϕ significantly below $\Omega_{\rm crit}$; dashed curves, RWM unstable plasma at $\omega_\phi/\Omega_{\rm crit} = 1$ with active feedback turned off; dotted curves, (upper two frames) actively stabilized plasma suffering a beta collapse from an internal $n = 2$ plasma mode. Shown are the evolution of (a) β_N, (b) ω_ϕ near $q = 2$, (c) current in representative nonaxisymmetric control coil, (d),(e) mode amplitude of $n = 1$ and 2 field components measured by the upper B_p sensor array, and (f) mode amplitude of $n = 1$ field component at the midplane, external to the vacuum vessel.

The reconstructed equilibrium at peak β_N of the actively stabilized, low-rotation plasma in Fig. 1, along with the positions of the copper stabilizer plates, RWM sensors, and mode control coils are shown in Fig. 2(a). There are 48 toroidally segmented stabilizer plates, covered with carbon tiles and arranged symmetrically in four toroidal rings, two above and two below the device midplane. Magnetic loops measuring the radial, B_r, and poloidal, B_p, flux are located at each of the plates closest to the midplane. The sensors are instrumented to detect modes with frequencies up to 2.5 kHz. There are 6 toroidally conformed, two-turn control coils mounted close to the machine vacuum vessel. This configuration is similar to midplane port module coil designs for ITER. Each coil nominally covers 60° of

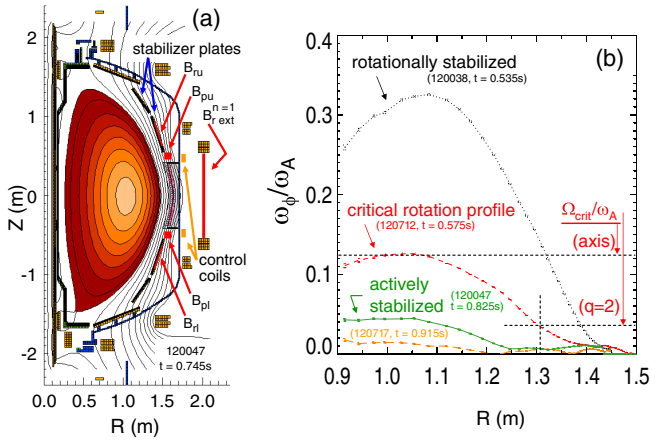

FIG. 2 (color online). Actively stabilized plasma equilibrium and rotation profiles. Shown are (a) NSTX cross section with poloidal flux contours, RWM sensor positions, and control coil locations; (b) ω_ϕ/ω_A vs R for plasmas that are rotationally stabilized, are at RWM marginal stability (critical rotation profile), and are actively stabilized below $\Omega_{\rm crit}$.

toroidal angle. In the present experiments, the coils are powered independently in three diametrically opposed pairs producing odd parity fields.

Plasma toroidal rotation profiles for several plasmas are shown in Fig. 2(b) at various times of interest. For comparison to studies of DIII-D and ITER, ω_ϕ is normalized to $\omega_A \equiv B_{\rm axis}/(R_{\rm axis}(\mu_0\rho)^{0.5})$, where $B_{\rm axis}$ and $R_{\rm axis}$ are the magnetic field at, and major radial position of, the magnetic axis and ρ is the local plasma mass density. The profile with peak $\omega_\phi/\omega_A = 0.325$ is from a rotationally stabilized plasma. The profile with peak $\omega_\phi/\omega_A = 0.125$ is from the plasma with no active stabilization in Fig. 1 at the time of RWM destabilization. It therefore defines the $\Omega_{\rm crit}/\omega_A$ profile. Note that at $q = 2$, $\Omega_{\rm crit}/\omega_A = 0.038$, compared to a value of 0.02 in DIII-D, consistent with the observed dependence of $\Omega_{\rm crit}/\omega_A$ on aspect ratio (Fig. 15 of Ref. [8]). The significantly reduced rotation profile of the actively stabilized plasma shown has $\omega_\phi/\Omega_{\rm crit} = 0.2$ at $q = 2$, and 0.3 at the magnetic axis. Comparing to predicted plasma rotation and critical rotation speeds for ITER advanced Scenario-4 plasmas [7], on-axis values are used, since a $q = 2$ surface does not exist in this ITER equilibrium. Reference [7] states that $\omega_\phi/\omega_A = 0.018$, and that $0.015 < \Omega_{\rm crit}/\omega_A < 0.03$ at the magnetic axis in ITER. Therefore, $1.2 < \omega_\phi/\Omega_{\rm crit} < 0.6$, and so the actively stabilized plasma in NSTX has $\omega_\phi/\Omega_{\rm crit}$ lower than ITER by at least a factor of 2. The ω_ϕ profile in Fig. 2 with the lowest values is from the actively stabilized plasma after the internal mode-induced β_N collapse and recovery (Fig. 1).

Variation of feedback control parameters for the active stabilization system demonstrated both positive and negative feedback response to the RWM. The measured $n = 1$ amplitude and phase, $\Delta B_{pu}^{n=1}$ and $\phi_{Bpu}^{n=1}$, are used to define the control coil currents,

$$I_A(\phi_{c(i)}, t) = G_p(t)\Delta B_{pu}^{n=1}(t)K_{c(i)}\cos(\phi_{c(i)} - \phi_{Bpu}^{n=1}(t) + \Delta\phi_f(t)) + I_{A0}(\phi_{c(i)}),$$

where subscript i represents coil number, G_p and $\Delta\phi_f$ are time-dependent gain and relative phase between the measured RWM amplitude and the control currents, $\phi_{c(i)}$ is the spatial toroidal phase offset for each of the control coils, $K_{c(i)}$ are calibration factors for each control coil, set to 69 A/G, and $I_{A0}(\phi_{c(i)})$ are time-dependent currents that do not depend on the measured RWM. The $\phi_{c(i)}$ are chosen to create a dominantly $n = 1$ magnetic field. The $I_{A0}(\phi_{c(i)})$ are chosen to create the $n = 3$ braking field. The effect of varying $\Delta\phi_f$ on the plasma is shown in Fig. 3(a) at $G_p = 1.0$. Choosing $\Delta\phi_f$ constant for each discharge, and varying from 45° through smaller angles, $\Delta B_{pu}^{n=1}$ shows an unfavorable positive feedback response for angles through 290°. With an unfavorable relative phase, $\Delta B_{pu}^{n=1}$ increases, leading to lower ω_ϕ, which in turn increases $\Delta B_{pu}^{n=1}$ if $\beta_N > \beta_N^{\rm no\text{-}wall}$, creating positive feedback and RWM instability. As $\Delta\phi_f$ is decreased, RWM instability is delayed, until at $\Delta\phi_f = 250°$ (same result at 225°) the plasma is actively stabilized. The plasma with $\Delta\phi_f = 225°$ suffers a partial β_N collapse due to an internal mode at $t = 0.765$ s. A damped response to this mode is observed in $\Delta B_{pu}^{n=1}$, indicating that control parameters are favorably set to produce negative feedback. The proportional gain G_p was also varied between 0.7 and 2.0 at $\Delta\phi_f = 225°$. Values up to $G_p = 1.5$ produced negative feedback, while equal or greater values resulted in a high frequency instability in the feedback control loop.

RWM stabilization can fail due to a change in the poloidal form of the mode. An example is shown in Fig. 3(b), where the $n = 1$ components of both upper and lower B_p and B_r sensors, and $\Delta B_{r-\rm ext}^{n=1}$ sensor signals are shown. Note that since the latter sensor is outside the

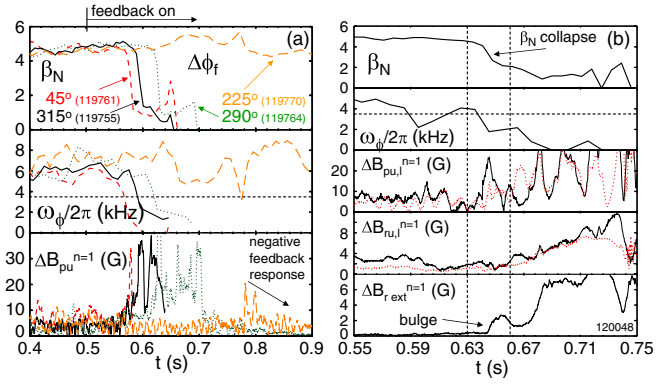

FIG. 3 (color online). Effect of feedback system relative phase on plasma stability [column (a)] and poloidal deformation leading to mode destabilization [column (b)]. Various relative phases are depicted by different line styles in column (a). In column (b), sensors are distinguished by solid (upper sensors) and dotted (lower sensors) lines.

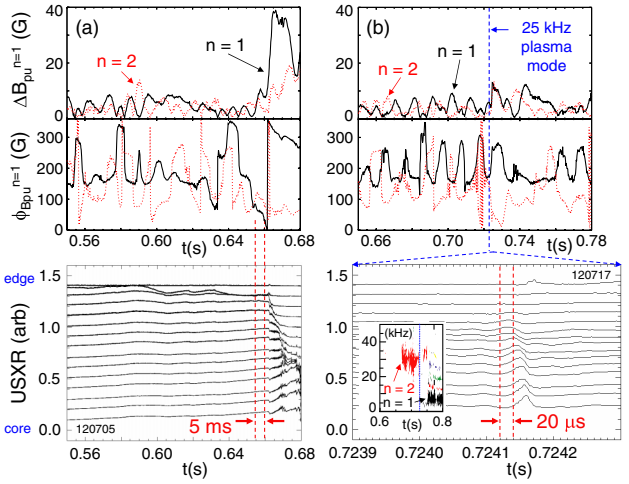

FIG. 4 (color online). Mode activity in plasmas with and without active stabilization. Frames from top down show upper B_p sensor amplitude, phase, and ultrasoft x-ray emission spanning from the plasma core to edge vs time. Solid lines, $n = 1$; dotted lines, $n = 2$. Column (a), discharge with active feedback off; column (b), RWM actively stabilized plasma with internal $n = 2$ plasma mode. Lower frame inset: n spectrum from midplane toroidal magnetic pickup coil array.

vacuum vessel, the signal lags those of the internal sensors by $\sim O(\tau_w) \sim 6$ ms for $n = 1$. Approaching the time of β_N collapse, $\Delta B_{pu}^{n=1}$ and $\Delta B_{pl}^{n=1}$ first decrease to near zero, as the radial field sensors increase by a small amount. Then, $\Delta B_{pu}^{n=1}$ increases strongly, while $\Delta B_{pl}^{n=1}$ lags, and the ratio $\Delta B_{pl}^{n=1}/\Delta B_{pu}^{n=1}$ never gets above 0.5. There is also a strong increase in $\Delta B_{r-\mathrm{ext}}^{n=1}$ while $\Delta B_{ru}^{n=1}$ and $\Delta B_{rl}^{n=1}$ decrease, indicating that the mode is bulging through the midplane gap in the stabilizing plates and decreasing in amplitude in front of the plates. This observation may indicate a lack of "mode ridigity," normally assumed theoretically and observed experimentally [11]. Similar behavior is observed under passive stabilization alone, indicating that the stabilizing plate geometry may play a role. The result has applicability to future devices with similar passive plate geometry, such as KSTAR. This poloidal deformation appears to occur when large I_A are requested and sometimes when the central q is near unity. These conditions may lead to nearby stable $n = 1$ MHD modes becoming less stable, causing the primary RWM eigenfunction to change poloidal structure.

The measured $n = 1$ and 2 RWM amplitude and phase, along with chord integrated soft x-ray (SXR) measurements spanning from the plasma core to the edge [21] are shown in Fig. 4. Without active stabilization, the $n = 1$ RWM becomes unstable. At early times in the figure, $\phi_{Bpu}^{n=1}$ appears to wobble between 150° and 300°, eventually settling to the lower end of this range, and as $\Delta B_{pu}^{n=1}$ grows exponentially, $\phi_{Bpu}^{n=1}$ shows mode rotation in the direction of plasma rotation, as expected by theory. SXR data show the mode amplitude largest in the outer region of the plasma, propagating toward the core during mode growth. The $n = 2$ RWM amplitude shows periods when $\Delta B_{pu}^{n=2} > \Delta B_{pu}^{n=1}$, but the $n = 2$ mode growth that eventually occurs, although strong, is subsidiary to $n = 1$ mode growth. Figure 4(b) shows analogous detail for the actively stabilized plasma suffering a largely internal mode shown in Fig. 1. Both $n = 1$ and 2 RWM activity is stable, with $\phi_{Bpu}^{n=1,2}$ wobbling within some range. SXR data show that mode growth on an ideal MHD time scale, much faster than τ_w, is largely internal, and the measured 25 kHz frequency indicates that the mode is $n = 2$, since it appears in a region of the plasma with $\omega_\phi/2\pi \sim 12$–15 kHz. The n spectrum measured by a toroidal array of magnetic pickup loops also shows $n = 2$ mode activity at this frequency and time.

The first RWM active stabilization experiments in low aspect ratio tokamak plasmas have demonstrated $n = 1$ RWM stabilization at low plasma rotation with direct applicability to future burning plasma experiments, including ITER. Stabilization of $n = 1$ did not lead to $n = 2$ RWM destabilization. Under certain conditions, the RWM is observed to deform poloidally, allowing destabilization. This may be due to the present combination of the stabilizing plate geometry and the location of sensors used for stabilization. Further study will assess the effect of using various sensor combinations on RWM active stabilization performance.

This research was supported by the U.S. Department of Energy under Contracts No. DE-FG02-99ER54524 and No. DE-AC02-76CH03073.

[1] A. Bondeson and D. J. Ward, Phys. Rev. Lett. **72**, 2709 (1994).
[2] E. J. Strait *et al.*, Phys. Rev. Lett. **74**, 2483 (1995).
[3] A. M. Garofalo *et al.*, Phys. Plasmas **9**, 1997 (2002).
[4] S. A. Sabbagh *et al.*, Nucl. Fusion **46**, 635 (2006).
[5] M. S. Chu *et al.*, Phys. Plasmas **2**, 2236 (1995).
[6] A. M. Garofalo *et al.*, Phys. Rev. Lett. **82**, 3811 (1999).
[7] Y. Liu *et al.*, Nucl. Fusion **45**, 1131 (2005).
[8] H. Reimerdes *et al.*, Phys. Plasmas **13**, 056107 (2006).
[9] M. Shimada *et al.*, Nucl. Fusion **44**, 350 (2004).
[10] A. M. Garofalo *et al.*, Nucl. Fusion **41**, 1171 (2001).
[11] M. Okabayashi *et al.*, Phys. Plasmas **8**, 2071 (2001).
[12] E. J. Strait *et al.*, Phys. Plasmas **11**, 2505 (2004).
[13] P. R. Brunsell *et al.*, Plasma Phys. Controlled Fusion **47**, B25 (2005).
[14] A. M. Garofalo *et al.*, Phys. Plasmas **9**, 4573 (2002).
[15] S. M. Kaye *et al.*, Nucl. Fusion **45**, S168 (2005).
[16] W. Zhu *et al.*, Phys. Rev. Lett. **96**, 225002 (2006).
[17] G. S. Lee *et al.*, Nucl. Fusion **41**, 1515 (2001).
[18] J. M. Bialek *et al.*, Phys. Plasmas **8**, 2170 (2001).
[19] S. A. Sabbagh *et al.*, Nucl. Fusion **41**, 1601 (2001).
[20] A. H. Glasser and M. C. Chance, Bull. Am. Phys. Soc. **42**, 1848 (1997); W. Newcomb, Ann. Phys. (Paris) **10**, 232 (1960).
[21] D. Stutman *et al.*, Rev. Sci. Instrum. **74**, 1982 (2003).